

Using Jet Substructure at the LHC to Search for the Light Higgs Bosons of the CP-Violating MSSM

Biplob Bhattacharjee^{a,1}, *Amit Chakraborty*^{b,2},
Dilip Kumar Ghosh^{b,3}, and *Sreerup Raychaudhuri*^{c,4}

^a Kavli Institute for the Physics and Mathematics of the Universe (WPI),
 The University of Tokyo, Kashiwa, Chiba 277-8583, Japan.

^b Department of Theoretical Physics, Indian Association for the Cultivation of Science,
 2A & 2B, Raja S.C. Mullick Road, Jadavpur, Kolkata 700 032, India.

^c Department of Theoretical Physics, Tata Institute of Fundamental Research,
 1, Dr. Homi Bhabha Road, Mumbai 400 005, India.

ABSTRACT

The CP -violating version of the Minimal Supersymmetric Standard Model (MSSM) is an example of a model where experimental data do not preclude the presence of light Higgs bosons in the range around 10 – 110 GeV. Such light Higgs bosons, decaying almost wholly to $b\bar{b}$ pairs, may be copiously produced at the LHC but would remain inaccessible to conventional Higgs searches because of intractable QCD backgrounds. We demonstrate that a significant number of these light Higgs bosons would be boosted strongly enough for the pair of daughter b -jet pairs to appear as a single ‘fat’ jet with substructure. Tagging such jets could extend the discovery potential at the LHC into the hitherto-inaccessible region for light Higgs bosons.

PACS Nos: 12.60.Fr, 14.80.Da, 13.85.Qk

¹E-mail: biplob.bhattacharjee@ipmu.jp

²E-mail: tpac@iacs.res.in

³E-mail: tpdkg@iacs.res.in

⁴E-mail: sreerup@theory.tifr.res.in

1 Introduction: Survival of Light Higgs Bosons

After four decades of relative stagnation, the physics of elementary particles has again reached a stage when empirical discoveries could lead the day. Theoretical structures built with much care and ingenuity over the previous decades now lie in serious danger of collapsing under the onslaught of data from the Large Hadron Collider (LHC). The most important of these theoretical structures under test is, of course, the Standard Model (SM) of particle physics. The first – and, it turns out, most stringent – test of the SM lies in the discovery of the predicted [1–4] Higgs boson H^0 . It is now universally known that a discovery has been made [5] of a boson of mass around 125 GeV which seems to resemble the Higgs boson of the SM [6], but further precise measurement of its couplings are required before it can be established as the SM Higgs boson in a manner convincing to all. The situation is expected to become much more clear at the end of the current year, after more data is collected and analysed.

Whatever be the outcome of these Higgs boson measurements, the issue of light Higgs bosons (i.e. masses $\lesssim 100$ GeV) will still remain wide open, so far as the LHC is concerned. This is because signals for a light Higgs boson decaying principally to b -jets will be completely swamped by the QCD background for production of $b\bar{b}$ pairs (and other dijets) – which is to say that such light Higgs bosons will be, for all practical purposes, invisible at the LHC. At a first reading, the above argument might seem to be purely academic, in view of the definite bound of $M_H \gtrsim 114.4$ GeV reported by the LEP-2 electroweak working group [7]. This is certainly true of the SM Higgs boson. However, we must remember that this bound arises from the negative results of searches for the Higgstrahlung process, viz.,

$$e^+ + e^- \rightarrow Z^* \rightarrow Z^0 + H^0 \rightarrow (\ell^+ \ell^-) + (b\bar{b}) \quad (1)$$

where $\ell = e, \mu$ or τ , and is, therefore, strongly dependent on the HZZ coupling. This coupling is, of course, fixed in the SM, and therefore the lower bound of 114.4 GeV is also fixed in the SM. On the other hand, any model with new physics beyond the SM (BSM) which can accommodate a significantly smaller HZZ coupling will immediately evade this bound. Thus, we can even now ask the question whether the observed new particle is the only Higgs boson, or is it one of a pack of scalars in some BSM physics model, where the others are invisible at the LHC because they are light?

Whenever new physics beyond the SM is indicated, the usual model of choice is the Minimal Supersymmetric Standard Model (MSSM) or one of its many variations. Even in the MSSM with all real and CP-conserving parameters, the lower bound on the lightest Higgs boson

mass (93 GeV for $\tan\beta > 6$) is different from that of the SM Higgs mass bound [8]. Not surprisingly, even this bound can be relaxed considerably in the presence of CP violation in the Higgs sector [9], where the lightest Higgs boson h^0 can have a substantial CP-odd component – which immediately implies a highly suppressed h^0ZZ coupling (see below).

Though an overwhelming majority of studies of the MSSM have assumed that the supersymmetric parameters are real and CP conserving, it may be recalled that of the 105 new undetermined parameters in the MSSM, only 62 of them are CP-conserving, while as many as 43 are CP-violating. Many of these CP-violating phases cannot be rotated away by simple re-definition of fields and this is known to lead to new sources of CP violation which may come in useful to explain the observed level of baryon asymmetry in the Universe [10]. However, these additional phases, especially those involving the first two generations, lead to large electric dipole moments (EDMs) of e^\pm and ν_e as well as of mercury (Hg) atoms – which come in conflict with the experimentally measured upper bounds on these EDMs [11–13]. The new CP phases may, therefore, be expected to be severely constrained. Fortunately, it turns out that such constraints are strongly dependent on the CP-conserving model parameters – specifically the nature of the mass spectrum involved in the calculation of those EDMs – and it has been explicitly shown that substantial cancellations among different EDM diagrams end up in allowing some combinations of the CP-violating phases to be large [14]. For example, the EDM constraints require the phase ϕ_μ of the higgsino mass parameter $\mu = |\mu|e^{i\phi_\mu}$ to be generally constrained to $\phi_\mu \lesssim 10^{-2}$ (unless we set the masses of all the sfermions very high). But if the sfermions of the first two generations are of the order of a few TeV [15] and we do not assume universality of the trilinear scalar couplings A_f [16, 17], then ϕ_μ can be considerably larger even if we keep the sfermions of the third generation light enough for easy detection at the LHC. The presence of CP-violating phases can substantially modify Higgs boson and superparticle production at colliders as well as decay modes and this has been the subject of several investigations [18] in the context of collider signals.

Though the new CP-violating phases appear only in the soft supersymmetry-breaking parameters μ , A_f and the three gaugino masses M_1 , M_2 and M_3 , some of them can induce CP violation at the one-loop level in the Higgs potential even if the tree-level Higgs potential is CP-conserving [19–24]. The quadratic terms for neutral states in this one loop-corrected Higgs potential can be written in terms of a 3×3 mass-squared matrix \mathcal{M}_{ab}^2 , where non-zero off-diagonal terms ($a \neq b$) involve mixing between scalar and pseudoscalar states. This is unlike the CP-conserving MSSM, where the scalar states (h^0 , H^0) and the pseudoscalar state A^0 do not mix. After diagonalisation, the physical neutral Higgs states h_1^0 , h_2^0 and h_3^0 (in

ascending order of mass) become admixtures of CP-even and CP-odd states. Since the pseudoscalar states do not couple to ZZ pairs, it is obvious that the $h_i^0 ZZ$ couplings ($i = 1, 2, 3$) arise only from the CP-conserving components of h_i^0 and therefore will be suppressed by the corresponding mixing angles. There exists enough freedom in choice of parameters in this CP-violating MSSM for at least some of these h_i^0 states to be light — which would make them invisible to conventional searches at the LHC. In fact, a set of benchmark points have been defined to showcase the maximal effect of CP violation in the MSSM Higgs sector, and this set goes by the name: ‘CPX scenario’ [23].

The LEP collaborations have searched for the processes

$$e^+e^- \rightarrow \begin{cases} Z^* \rightarrow Z^0 + h_i^0 \rightarrow \ell^+\ell^- + b\bar{b} & (i = 1, 2, 3) \\ h_1^0 + h_2^0 \rightarrow 4b \\ h_1^0 + h_2^0 \rightarrow 3h_1^0 \rightarrow 6b \\ Z^0 + h_2^0 \rightarrow Z^0 + 2h_1^0 \rightarrow (\ell^+\ell^-) + 4b \end{cases}$$

in the CP-violating MSSM Higgs sector based on the CPX scenario [25]. For certain choices of CP-violating parameters within the CPX scenario, the LEP-2 data allow for a much lighter Higgs boson h_1^0 with a mass $M(h_1) \approx 40\text{--}50$ GeV [8, 26, 27] because, as expected, there are very substantial reductions in the $h_1^0 ZZ$ coupling [23]. It turns out that for the selfsame sets of parameters the couplings $h_1^0 WW$, $h_1^0 ZZ$ and $h_1^0 t\bar{t}$ all get reduced simultaneously, as a result of which none of the canonical search channels for h_1^0 at the Tevatron and LHC are expected to be viable [26, 28–30]. This implies that there is a ‘blind spot’ or ‘hole’ in the parameter space which is permitted by all experimental data till date. Different search strategies in the future runs of the LHC have been proposed to close this ‘blind spot’ [28, 31–33]. These have varying levels of success, depending on the specific choice of parameters, but none can be said to be the definitive search strategy for light Higgs bosons belonging to this inaccessible region.

In this work, we explore a method of searching for these light Higgs bosons which is based essentially on kinematics, and hence is not overly sensitive to the parameter choices of the theory. Our strategy is to apply to the case of the light Higgs bosons of the CP-violating MSSM some of the techniques developed recently for tagging a heavy boosted particle decaying to a single fat jet with substructure [34–39]. Since the h_1^0 , h_2^0 and h_3^0 can all decay to a pair of highly-boosted b -jets, one could ask if this technique can suitably identify the Higgs boson states over and above the enormous QCD background at the LHC. Daunting as the task may seem at first, we demonstrate that this technique, in fact, works quite well, and can be considered as an important probe of the CP-violating Higgs sector.

The basic technique can, in fact, be used in the wider context of light scalar states, such as those considered recently in Ref. [40].

2 The Higgs Sector of the CP-violating MSSM

As already mentioned in the introductory section, the non-vanishing phases of μ and/or the trilinear scalar couplings A_t and A_b can induce explicit CP violation in the Higgs sector. Since the only Yukawa interactions of the Higgs bosons which can have any significant effects are those to top and bottom squarks, this feature is reflected in the trilinear couplings as well, and thus the only relevant CP phases are $\phi_\mu = \text{Arg}[\mu]$, $\phi_t = \text{Arg}[A_t]$ and $\phi_b = \text{Arg}[A_b]$. Given these, the scalar potential, even though invariant under CP-transformation at tree level, receives CP-violating contributions through one-loop corrections.

We briefly review the formalism required to include CP-violating effects in the MSSM. As is usual, we write the two scalar doublets as gauge eigenstates in the form

$$\Phi_1 = \begin{pmatrix} \phi_1^+ \\ \phi_1^0 + i\eta_1^0 \end{pmatrix} \quad \Phi_2 = \begin{pmatrix} \phi_2^0 + i\eta_2^0 \\ \phi_2^- \end{pmatrix} \quad (2)$$

Once we allow the parameters in the scalar potential to have CP-violating phases, the mass matrix for the neutral scalars assumes the general form

$$\mathcal{L}_{\text{mass}} = \left(\begin{array}{cc|cc} \eta_1^0 & \eta_2^0 & \phi_1^0 & \phi_2^0 \end{array} \right) \left(\begin{array}{c|c} \mathcal{M}_P^2 & \mathcal{M}_{SP}^2 \\ \hline \hline [\mathcal{M}_{SP}^2]^T & \mathcal{M}_S^2 \end{array} \right) \begin{pmatrix} \eta_1^0 \\ \eta_2^0 \\ \phi_1^0 \\ \phi_2^0 \end{pmatrix} \quad (3)$$

This 4×4 mass matrix is partitioned into 2×2 blocks, with independent \mathcal{M}_P^2 , \mathcal{M}_S^2 and \mathcal{M}_{SP}^2 — of which the last is absent in the CP-conserving MSSM but is generated in the CP-violating MSSM through the one-loop corrections mentioned above [19–24]. The magnitude of different contributions to the terms in the 2×2 matrix \mathcal{M}_{SP}^2 may be estimated as [20]:

$$\mathcal{M}_{SP}^2 \approx \mathcal{O} \left(\frac{M_t^4 |\mu| |A_t|}{v^2 32\pi^2 M_{\text{SUSY}}^2} \right) \sin \Phi_{\text{CP}} \times \left[6, \frac{|A_t|^2}{M_{\text{SUSY}}^2}, \frac{|\mu|^2}{\tan \beta M_{\text{SUSY}}^2}, \frac{\sin 2\Phi_{\text{CP}} |A_t| |\mu|}{\sin \Phi_{\text{CP}} M_{\text{SUSY}}^2} \right] \quad (4)$$

where $\Phi_{\text{CP}} = \text{Arg}(A_t \mu)$, $v = 246$ GeV. and the mass scale M_{SUSY} is defined by

$$M_{\text{SUSY}}^2 = \frac{m_{\tilde{t}_1}^2 + m_{\tilde{t}_2}^2}{2}. \quad (5)$$

Rough estimates of the degree of CP violation in the Higgs sector can be formed by taking the dominant one(s) of these contributions. For example, from the above expression it is clear that a sizeable scalar-pseudoscalar mixing is possible for a large CP-violating phase Φ_{CP} , $|\mu|$ and $|A_t| > M_{\text{SUSY}}$.

The diagonalisation of this 4×4 mass-squared matrix can be carried out in two stages, of which the first is to simply diagonalise the sub-matrix \mathcal{M}_P^2 and replace the pseudoscalars η_1^0, η_2^0 with the more familiar G^0, A^0 . It turns out that after this is done, the first row and column of the 4×4 mass matrix are left only with contributions from tadpole diagrams, which would be removed in any renormalisation programme. It follows that, apart from a massless Goldstone boson G^0 which does not mix further with the other neutral states and is eventually absorbed by the massive Z^0 boson, we obtain a 3×3 Higgs mass-squared matrix \mathcal{M}^2 , with a mass term

$$\mathcal{L}_{\text{mass}} = \begin{pmatrix} A^0 & \phi_1^0 & \phi_2^0 \end{pmatrix} \begin{pmatrix} \mathcal{M}_{ij}^2 \end{pmatrix} \begin{pmatrix} A^0 \\ \phi_1^0 \\ \phi_2^0 \end{pmatrix} \quad (6)$$

where A^0 is the appropriate eigenstate of \mathcal{M}_P^2 . Diagonalising this 3×3 symmetric matrix \mathcal{M}_{ij}^2 by an orthogonal matrix \mathcal{O} ,

$$\begin{pmatrix} h_3^0 \\ h_2^0 \\ h_1^0 \end{pmatrix} = \begin{pmatrix} \mathcal{O}_{ij} \end{pmatrix} \begin{pmatrix} A^0 \\ \phi_1^0 \\ \phi_2^0 \end{pmatrix} \quad (7)$$

we see that the physical mass eigenstates h_1^0, h_2^0 and h_3^0 (in ascending order of mass) are mixtures of the CP-odd A^0 and the CP-even ϕ_1^0 and ϕ_2^0 . These, therefore, are states of indefinite CP. The usual sum rules for neutral Higgs boson masses (i.e. eigenvalues of \mathcal{M}^2) become much more complicated than in the CP-conserving case. Moreover, as A^0 is no longer a physical state, the charged Higgs boson mass M_{H^\pm} is a more appropriate parameter for description of the MSSM Higgs-sector in place of the M_A used in the CP-conserving model.

The coupling of these new states h_i^0 ($i = 1, 2, 3$) to the weak gauge bosons W^\pm and Z^0 will obviously be different from those in the CP-conserving MSSM. We can write them as [20]

$$\begin{aligned} \mathcal{L}_{hVV}^{\text{int}} &= gM_W \sum_{i=1}^3 g_{h_i VV} \left(h_i^0 W_\mu^+ W^{-,\mu} + \frac{1}{2 \cos^2 \theta_W} h_i^0 Z_\mu Z^\mu \right) \\ \mathcal{L}_{hhZ}^{\text{int}} &= \frac{g}{2 \cos \theta_W} \sum_{i,j=1}^3 g_{h_i h_j Z} (h_i^0 \overset{\leftrightarrow}{\partial}_\mu h_j^0) Z^\mu + \text{H.c.} \end{aligned}$$

$$\mathcal{L}_{hH^\mp W^\pm}^{\text{int}} = \frac{g}{2 \cos \theta_W} \sum_{i=1}^3 g_{h_i H^+ W^-} (h_i^0 \overset{\leftrightarrow}{\partial}_\mu H^+) W^{-,\mu} + \text{H.c.} \quad (8)$$

where

$$\begin{aligned} g_{h_i VV} &= \mathcal{O}_{1i} \cos \beta + \mathcal{O}_{2i} \sin \beta \\ g_{h_i h_j Z} &= \mathcal{O}_{3i} (\cos \beta \mathcal{O}_{2j} - \sin \beta \mathcal{O}_{1j}) - (i \leftrightarrow j) \\ g_{h_i H^+ W^-} &= \mathcal{O}_{2i} \cos \beta - \mathcal{O}_{1i} \sin \beta + i \mathcal{O}_{3i} \end{aligned} \quad (9)$$

These couplings obey the following sum rules:

$$\sum_{i=1}^3 g_{h_i VV}^2 = 1, \quad g_{h_i VV}^2 + |g_{h_i H^+ W^-}|^2 = 1, \quad g_{h_k VV} = \epsilon_{ijk} g_{h_i h_j Z} \quad (10)$$

from which one can see that if two of the $g_{h_i^0 ZZ}$ are known, then the whole set of couplings of the neutral Higgs boson to the gauge bosons are determined. It is interesting to see from Eqn. (10) that in the case of large scalar-pseudoscalar mixing the suppressed $h_1^0 VV$ coupling means an enhanced $h_1^0 H^+ W^-$ coupling. This has been exploited to develop search strategies in Ref. [31, 32].

Having described the formalism in which one can study the mixed CP Higgs bosons of the model, we require to choose the parameters of interest. We use the package CPSUPERH(version 2.2) [41] to generate the entire particle spectrum of the CP-violating MSSM for every given set of input parameters. It has already been mentioned that the quantity $\sin \Phi_{\text{CP}}/M_{\text{SUSY}}^2$ needs to be large to support significant CP-mixing in the Higgs sector. As mentioned in the introductory section, the benchmark scenario dubbed the ‘CPX scenario’ [23] nicely showcases this CP violation since, among other things, it makes the $h_1^0 ZZ$ coupling small enough to evade the LEP bounds [8, 26, 27]. This CPX scenario may be summarised as the specific parameter choices

$$\begin{aligned} M_{\tilde{Q}} = M_{\tilde{t}} = M_{\tilde{b}} = \frac{\mu}{4} = \frac{|A_t|}{2} = \frac{|A_b|}{2} = \frac{|A_\tau|}{2} &= M_{\text{SUSY}} \\ \text{Arg}[A_t] = \text{Arg}[A_b] = \text{Arg}[A_\tau] & \end{aligned} \quad (11)$$

It is important to note that this is just a benchmark scenario which allows us to find parameter choices which lie in the ‘blind spot’ or inaccessible region of previous collider experiments, and does not exhaustively cover the whole of the inaccessible parameter space. However, it suffices to provide a framework for predicting the existence of light, hitherto-invisible Higgs bosons, which is the subject of this work. In fact, instead of exploring the entire CPX scenario and its manifold variations, we find that it is sufficient to choose four benchmark points BP-1, BP-2, BP-3 and BP-4, and concentrate our exploratory studies on these points.

We use the well-known code HIGGSBOUNDS (version 2.1.1) [42] to ensure that these four benchmark points are allowed by the LEP-2 and Tevatron Higgs searches. The choice of parameters common to all the four benchmark points (BP) are as follows:

- $M_{\text{SUSY}} = 500$ GeV and $\Phi_{\text{CP}} = \text{Arg}[A_t] = \text{Arg}[M_{\tilde{g}}] = \pi/2$. The related parameters are then fixed using Eqn. (11).
- The remaining phases are fixed as $\text{Arg}[M_1] = \text{Arg}[M_2] = 0$.
- The gluino mass is fixed to $M_{\tilde{g}} = 1.2$ TeV, as are the masses of squarks of the first two generations; the squarks of the third generation are assumed to have masses 500 GeV.
- The top quark mass is taken to be 173.13 GeV [44]. Of course, this is not a free parameter, but its exact value determines the top Yukawa coupling and hence controls the running of SUSY masses and couplings between the SUSY-breaking scale and the electroweak scale in a critical manner.

The parameters which differ from one benchmark point to another are given in Table 1, where a vertical line separates these input parameters from some masses calculated by the CPSUPERH package.

BP	M_1	M_2	$\tan\beta$	$M(H^\pm)$	$M(h_1^0)$	$M(h_2^0)$	$M(h_3^0)$	$M(\tilde{\chi}_1^0)$	$M(\tilde{\chi}_1^\pm)$
1	100	200	6	125.7	49.4	101.8	130.4	99.7	198.6
2	100	200	15	128.0	68.3	111.6	125.1	99.8	199.2
3	200	400	15	130.0	72.1	113.2	125.8	199.8	398.9
4	100	200	8	140.0	83.0	112.7	135.6	99.7	198.9

Table 1: Our choice of benchmark points in the CPX scenario. In addition to the parameter choices, we present the masses of the three neutral Higgs states h_1^0 , h_2^0 and h_3^0 , as well as the lightest neutralino $\tilde{\chi}_1^0$ and the lightest chargino $\tilde{\chi}_1^\pm$. The next-to-lightest neutralino $\tilde{\chi}_2^0$ is almost degenerate with the $\tilde{\chi}_1^\pm$. All masses are in units of GeV.

This table illustrates very well some of the points made in the previous discussion. They have the common feature that the lightest Higgs boson is much lighter than the LEP bound and will therefore be highly boosted at the LHC. It is interesting that for BP-2 and BP-3, the third of the neutral Higgs bosons lies precisely in the range where the new boson has been found [5], but it would be premature to read too much into this until we have a precise measurement of the couplings. Similarly we do not concern ourselves overly with the relatively light charged Higgs bosons, although they do make substantial contributions [45] to the decay width for the process $B_s \rightarrow \mu^+ \mu^-$. In fact, strictly speaking, if we take the current upper bounds from the LHCb on this branching ratio [46], none of our benchmark points

would be tenable⁵. For the moment, however, our interest focuses on the light Higgs bosons h_1^0 (and sometimes the h_2^0), where we shall presently show that tagging of their boosted decay products can help their detection at the LHC, and thereby shed some light on the parameter space which has hitherto been a ‘blind spot’ for collider experiments.

3 Boosted Higgs Bosons and Jet Substructure

In this section we discuss the technique used to identify light Higgs bosons decaying into a pair of b -jets over and above the enormous QCD background. This is a technique based essentially on kinematics and hence is not specific to any model. The CP -violating MSSM described in the previous section acts here only as a phenomenologically-viable framework which can support the existence of light Higgs bosons.

The study of jet substructure began some years ago [34–39] with the realisation that in searches for new physics, the kinematic configuration of final states involving hadronic jets at the LHC can be very different from those studied earlier at colliders operating close to the electroweak scale, such as the LEP (91 – 205 GeV), the Tevatron (around 300 – 350 GeV) and the HERA (200 – 300 GeV). At these machines, the major searches were for new particles of mass between some tens of GeV to a few hundred GeV, i.e. the masses were comparable to the machine energy. When particles of such mass are produced, they do not carry much momentum and hence are only mildly boosted. At the LHC, however, the available centre-of-mass energy is around 1 – 2 TeV, but the particles being sought are the same as before. It follows, therefore, that, if produced, these particles will be very highly boosted. This realisation has led to a new paradigm for studies of new physics in hadronic final states at the LHC. In fact, if a new particle of mass in the range of a few hundred GeV is discovered at the LHC then further studies of that particle would almost always include a strong boost. It may be kept in mind, however, that if new physics continues to elude LHC searches, the mass limits on these particles will eventually increase and become comparable to the available machine energy — thereby restoring the situation at earlier colliders and reinstating the techniques invented for those specific studies. The present study (and all similar studies) are, therefore, currently relevant because we are in the early stages of the LHC run.

⁵However, this can be circumvented in various ways, either by going beyond the minimal flavour violation paradigm, or by activating some of the supersymmetric phases set to zero in our choice of benchmark points, without prejudice to the existence of light neutral Higgs states. This issue will be taken up in a future work [47].

The main feature of the decay products of a boosted particle decaying into multiple hadronic jets is that the final states remain highly collimated, appearing as a single fat jet. Thus, at the LHC, there will be W/Z -jets [34, 35, 48], t -jets [37, 38, 43] and H -jets [36, 49] in the Standard Model, and in new physics models there will be objects like charged Higgs jets [50], neutralino jets [51], etc., depending on the model chosen. The invariant mass of such a jet, constructed by adding the momenta of all the hadronic clusters, will peak at the mass of the parent particle, i.e. at M_W , M_Z , m_t , and so on. However, it is not enough to identify fat jets with a certain range of invariant mass, since there will be a substantial QCD background to these – enough to mask the small numbers due to production of these heavier particles. It is necessary, therefore, to tag the fat jets further by scanning them at higher angular resolutions for substructures which would betray their origin from the decay of heavy particles, rather than a series of gluon radiations and gluon splittings, which characterises the typical QCD jet. Criteria imposed on the substructure of fat jets have been used with success to tag W , Z and t jets, and here we apply a set of such criteria designed to identify fat jets arising from light Higgs bosons decaying to a pair of b quarks.

The exact method used by us to tag Higgs boson jets closely follows that used in Ref. [36]. We now describe this technique, which has three stages. In our numerical simulation the basic processes are calculated using the well-known Monte Carlo generator PYTHIA [52], and the jets are identified using the add-on package FASTJET [53]. Thus, we start with a bunch of hadronic final states, of which some are identifiable with known hadrons, but others are just clumps of quarks and gluons, bound together for some short lifetimes. This is the theoretical equivalent of what the experimentalist would see as a bunch of hadronic ‘clusters’ recorded in the hadron calorimeter (HCAL). As the first stage in our analysis, we identify a jet from these putative ‘clusters’, by applying the Cambridge/Aachen (C/A) algorithm [54], which operates as follows.

- The angular distance ΔR_{ij} between all pairs (i, j) of ‘clusters’ is given by

$$\Delta R_{ij} = \sqrt{(y_i - y_j)^2 + (\varphi_i - \varphi_j)^2} \quad (12)$$

where $y_i = \frac{1}{2} \ln(E_i - p_{Li}) / (E_i + p_{Li})$ is the rapidity and φ_i is the azimuthal angle of the i^{th} cluster. This quantity, which is invariant under longitudinal boosts, is tabulated for all pairs (i, j) and the pair with the smallest value of ΔR_{ij} is merged into a single ‘cluster’, i.e. the momentum four vectors are added into a single momentum four vector. We thus have a new configuration with one less ‘cluster’ than before.

- The above exercise is then repeated with the new configuration, as a result of which the number of ‘clusters’ is again reduced by unity. This is iterated until there remains only

a single four vector which has been built up by this merging process, with the nearest hadronic ‘cluster’ lying at an angular distance $\Delta R > R_0$, where R_0 is a predetermined angular width for a ‘fat’ jet. The synthetic four vector (P, M) built up by this process is identified as that of a jet, and the three-momentum \vec{P} of this jet is identified as the jet axis. The invariant mass of this jet is simply constructed by taking $M = \sqrt{P_0^2 - \vec{P}^2}$. For Higgs boson masses in the range of a few tens of GeV the entire Higgs jet algorithm works best if we set $R_0 = 0.6$ and this is what is done in the rest of the discussion.

- One then iterates the above procedure for all hadronic clusters lying outside the cone $\Delta R = R_0$ centred around this jet axis, i.e. for this part of the study, the four-vector already identified as a jet will be excluded. It is likely that the remaining clusters will again combine to form a different jet under this algorithm, or more than one jet, as the iterative process continues.
- Some of the jets thus synthesised may be soft, with P_T lying below 20 GeV. These are usually discounted and only hard jets ($P_T > 20$ GeV) thrown up by the C/A algorithm are involved in the remaining part of the analysis.

The C/A algorithm described above⁶ generically leads to a multi-jet final state depending on the number and configuration of hadronic ‘clusters’. Of course, this algorithm will indiscriminately pick up QCD jets as well as those arising from heavy particle decay, so it should be considered only as the initial step in our search for heavy particle jets. In order that the next step be possible, the merging history must be stored for every hard ‘fat’ jet created by the C/A algorithm. In the second stage of our analysis, this history is then used to (partially) eliminate QCD jets by *reversing* the process of synthesis and applying the following criteria at the different stages of the reversal:

- The jet — read four-momentum (P, M) — is broken into two sub-jets (p, m) and (p', m') by reversing the last merging performed in the C/A synthesis, which means that $P = p + p'$. The ordering should be such that $M \geq m > m'$.
- We then check the ‘mass drop’ i.e. if $m' < xM$ (where x is a smallish fraction), then it is likely that the corresponding softer sub-jet was a radiated gluon. Following Ref. [36], we set $x = \frac{1}{3}$. There are two cases, viz.

⁶Many experimental analyses prefer to apply the so-called k_T and anti- k_T algorithms, where the C/A distance function ΔR_{ij} is modified by a momentum-dependent factor. For the present analysis, the anti- k_T algorithm would not work at all, and there is no practical advantage to be gained by the k_T algorithm. Hence, we confine ourselves to the simpler C/A algorithm.

1. If $0 < m' < xM$, then we eliminate the final step in the merging and zero in on the harder sub-jet with (p, m) and start again, i.e. we consider the previous step in which (p, m) was formed by the merging of two ‘clusters’, and repeat this analysis. For all practical purposes, the softer sub-jet with (p', m') forms no part of the remaining analysis.
2. If $xM < m' < M$, then we assume that we have found two sub-jets of comparable momenta and further apply a symmetry criterion. This amounts to calculating ΔR between the two sub-jets and constructing

$$y = \frac{\min(p_T^2, p_T'^2)}{m'^2} \Delta R^2 \approx \frac{\min(p_T^2, p_T'^2)}{\max(p_T^2, p_T'^2)} \quad (13)$$

The symmetry criterion is then set Ref. [36] as $y > 0.09$, which is consistent with the value of x chosen before. In practice, passing both these criteria simply means that we are satisfied that the sub-jets arise from decay of a heavy particle (as opposed to a gluon radiation/splitting) if they share the energy and momentum of the composite ‘fat’ jet in a ratio not more skewed than 2:1.

- The final step in identifying a ‘Higgs jet’ would be to demand that the two reasonably symmetric sub-jets picked out by the above algorithm are tagged as b -jets. For the experimentalist, this would mean that these jets correspond to displaced vertices in the tracker. However, in a theoretical analysis, we have the luxury of knowing the exact components of each sub-jet, whose history can be tracked down to the parton level even before fragmentation. Thus, we can achieve virtual b -tagging simply by looking for a b -quark parentage for the sub-jets in question. This process, however, has a 100% efficiency and a very small mistagging fraction, both of which are unrealistic. We therefore require to import proper efficiency criteria from the existing experimental analyses (see below).

The above criteria are fairly efficient in eliminating QCD jets, but are not so efficient in eliminating jets arising from underlying events – which are again a new problem at the enhanced energies and luminosities of the LHC. If these are not filtered out, the Higgs boson mass reconstruction is adversely affected. We note that the b sub-jets will have an angular separation given approximately by $R_{b\bar{b}} \gtrsim 2M_H/p_T^H$ – which is smallish for boosted Higgs bosons, but much larger than the angular resolution of the ATLAS and CMS detectors. Although the cross section for $b\bar{b}$ pairs from underlying events will scale as $(R_{b\bar{b}})^4$ [55], it turns out that for Higgs masses around 100 GeV and $p_T \sim 200 - 300$ GeV, $R_{b\bar{b}}$ is not so small that underlying events can be neglected. Therefore, there is a third stage to our analysis,

where the Higgs jet candidates picked out by the previous algorithm are subjected to a ‘filtering’ process. This works as follows.

- Working back as before, we decompose the constituents of the candidate jet into the original hadronic ‘clusters’. Other jets and stable final states remain untouched.
- We define a new angular criterion r_0 , and re-run the C/A algorithm to identify sub-jets with this criterion instead of R_0 . Again following Ref. [36], we set $r_0 = 0.2$. However, as a check, we tried different values of this cone radius, viz. $r_0 = 0.1, 0.2, 0.3$ etc. For Higgs bosons in the mass range of interest, the maximum efficiency in choosing candidates for light Higgs bosons occurs for the choice $r_0 = 0.2$, and this is what we present our results for.
- Of all the sub-jets thrown up by the above algorithm we choose the three hardest and eliminate all the others. Of these three sub-jets, if the hardest two are b -tagged, we identify the jet as a Higgs boson candidate. Note that we take three hard sub-jets in order not to lose the not-so-rare $H \rightarrow b\bar{b}g$ events.

The above filtering process removes rare QCD cases where a very hard gluon is radiated, as well as hard emissions from underlying events, which could have satisfied the criteria in the first two stages, but will fail the last one. Once these three stages of identification are passed, we can be sure that a reasonable fraction of the tagged jets will originate from Higgs bosons. Our next step, therefore, is to see how efficient this Higgs jet-finding algorithm can be.

To make a specific study, we have made a Monte Carlo simulation of the following exclusive process:

$$\begin{aligned}
 p + p &\rightarrow \tilde{\chi}_2^0 + \tilde{\chi}_1^0 \\
 &\hookrightarrow \tilde{\chi}_1^0 + h_1^0
 \end{aligned}
 \tag{14}$$

where the branching ratio for $\tilde{\chi}_2^0 \rightarrow \tilde{\chi}_1^0 + h_1^0$ is set to unity. The masses of the neutralinos $\tilde{\chi}_1^0$ and $\tilde{\chi}_2^0$ are set to 100 GeV and 700 GeV respectively in this toy model, and all other processes are switched off. The masses of the $\tilde{\chi}_1^0$ and $\tilde{\chi}_2^0$ are chosen so as to have a sufficient phase space for the Higgs boson to be produced with a large p_T . It may be noted that it was not essential to have a supersymmetric origin of the Higgs bosons – a Higgstrahlung process $p + p \rightarrow Z^0 + h_1^0$, with subsequent decay of $Z^0 \rightarrow \nu\bar{\nu}$, would have yielded the same final state, where we have only h_1^0 particles decaying to $b\bar{b}$ pairs in addition to other incidental debris from effects like initial state radiation, final state radiation, multiple interactions, and, of course, a great deal of missing energy and momentum. However, the processes in Eqn. (14)

are preferred since they permit us to study a larger range in p_T for the Higgs boson than the Higgstrahlung process would have allowed. In this simulation, the mass of the Higgs boson h_1^0 is varied over the range 20 – 150 GeV and the p_T is noted. A total of 50 000 ‘events’ was simulated for every value of $M(h_1)$. For every bin in $p_T(h_1)$, we apply the jet-finding algorithm described above in all its three stages and note the efficiency, i.e the ratio of the number actually tagged as Higgs jets to the original number of h_1^0 produced. This enables us to produce the contour plots of Figure 1.

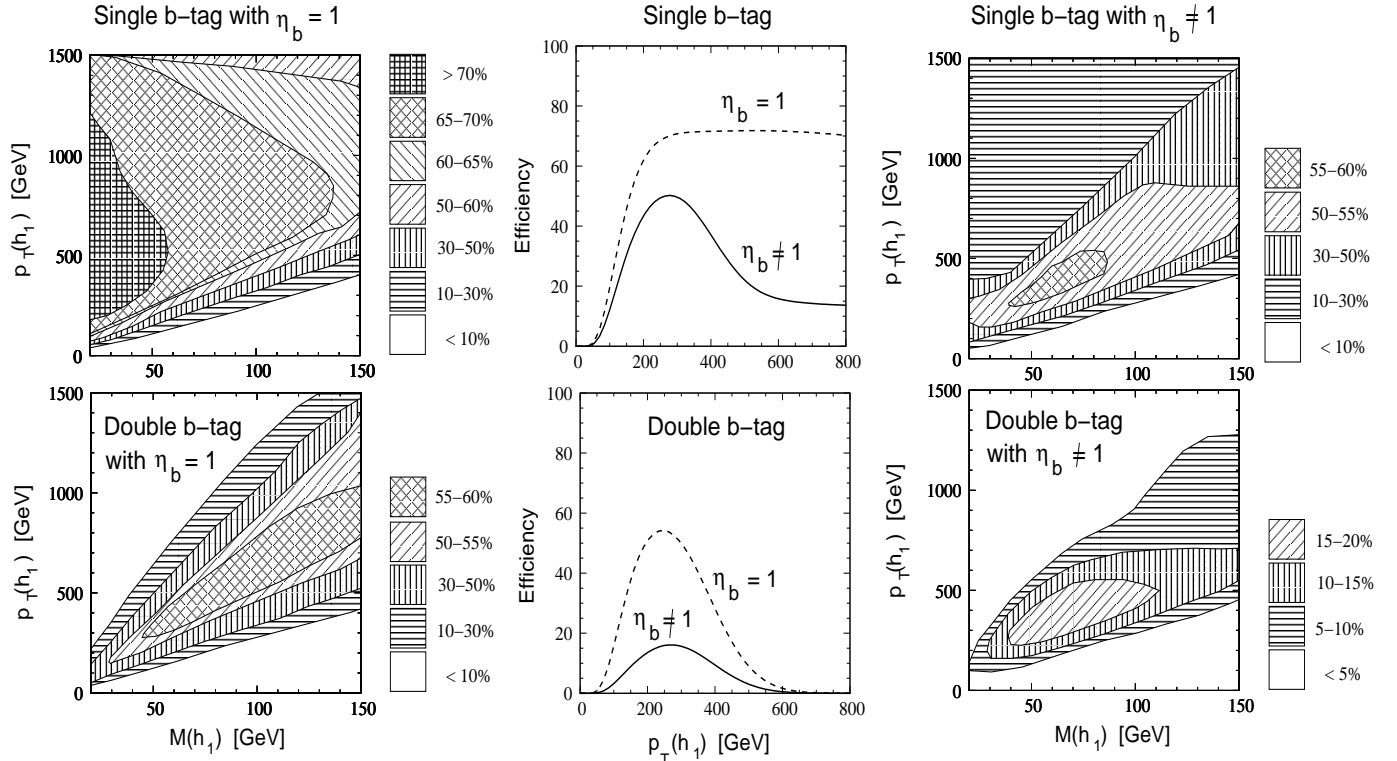


Figure 1: Illustrating the efficiency of Higgs-tagging of ‘fat’ jets by the method described in this section. The upper (lower) row of panels corresponds to a single (double) b -tag among the sub-jets thrown up by the ‘filtering’ algorithm. The two panels on the left illustrate contours of the efficiency of this algorithm in the plane of $p_T(h_1)$ versus $M(h_1)$ assuming b -tagging is perfect. The panels in the middle show the effect, for $M(h_1) = 100$ GeV, of including the b -tagging efficiency with its p_T -dependence. The panels on the right show the results of convolution of the b -tagging efficiencies with those shown in the panels on the left, thereby producing a more-or-less realistic estimate of the actual efficiencies obtainable at the LHC.

Some explanation of the plots in Figure 1 is required at this stage. Let us first consider the upper row of panels in Figure 1. We start with the upper panel on the extreme left, labelled ‘Single b -tag with $\eta_b = 1$.’ This shows the result of implementation of the above algorithm with just one difference: after ‘filtering’, we pick up three hard jets and of the hardest two, only one is required to have a b -tag. The plot shows contours of efficiency for the Higgs-jet finding algorithm, with the b -tagging efficiency set to unity. It may be seen that for a given

Higgs mass $M(h_1)$, the efficiency is small for small p_T , increases as p_T increases, and then falls again as p_T increases to very large values. This behaviour is exactly what one would expect as the boost parameter increases. When the boost is very small, the jets arising from Higgs boson decay tend to be widely separated, and hence jets found within a cone of radius $R_0 = 0.6$ will not show any substructure, as they essentially arise from the decay of a single b -quark. As the boost increases, more of the jets will now get collimated and we will begin to see the phenomenon of a fat jet with substructure, to which the finding algorithm is tuned. Not surprisingly, the efficiency will increase in this regime. However, when the boost is very large, the final states will form a very thin pencil and it may not be possible to resolve individual sub-jets using the criterion $r_0 = 0.2$. In this case, the efficiency will again fall. Increase in the Higgs mass $M(h_1)$ is equivalent to scaling down the p_T , and this is reflected in the contours shown in the figure. It augurs well for the success of this method that there is a substantial range of Higgs mass and Higgs p_T where the efficiency can be as high as 70% or above, and that much of the $p_T(h_1)$ – $M(h_1)$ plane corresponds to an efficiency of 50% or more.

As mentioned before, it is unrealistic to take the b -tagging efficiency as $\eta_b = 1$. Following the experimental collaborations [56], we choose the p_T -dependent efficiency as

$$\eta_b = \begin{cases} 0 & \text{for } p_T^b \leq 20 \text{ GeV} \\ 0.3 & \text{for } 20 \text{ GeV} < p_T^b \leq 50 \text{ GeV} \\ 0.6 & \text{for } 50 \text{ GeV} < p_T^b \leq 400 \text{ GeV} \\ 0.2 & \text{for } p_T > 400 \text{ GeV} \end{cases}$$

This must be convoluted with the non-realistic efficiency shown in the upper left panel of Figure 1, to obtain a more realistic picture. The results of such a convolution are shown in the central upper panel, marked ‘Single b -tag’ for $M(h_1) = 100$ GeV. Here, it is easy to see how the efficiency is reduced quite dramatically by the requirement of b -tagging. What we gain in return, of course, is a much sharper drop in the background (not shown). The panel on the upper right of Figure 1, which is marked ‘Single b -tag with $\eta_b \neq 1$ ’, shows the contours of Higgs tagging efficiency after convolution with the b -tagging efficiency. This is a much more realistic estimate of the efficiency, where one notes that the poorer results at high p_T arise because of the weakness of the b -tagging algorithm in that regime. There is still, however, a substantial range of Higgs mass and p_T where the efficiency is 30% or more, and this is enough for the Higgs tagging algorithm to yield positive results, as we shall presently demonstrate.

Obviously, if we demand that *both* the harder sub-jets be b -tagged, we will get even lower

efficiencies. The advantage, on the other hand will be to have almost negligible mistagging probabilities. The lower three panels in Figure 1 illustrate the efficiency obtained by tagging both b -sub-jets. On the left, we plot contours of efficiency for a ‘Double b -tag with $\eta_b = 1$ ’, where efficiencies above 55% may be achieved in the optimum range of Higgs mass and transverse momentum. The central panel, marked ‘Double b -tag’ illustrates, like the panel above it, the effect of implementing realistic b -tagging on the efficiency contours for $M(h_1) = 100$ GeV. Not only does the overall efficiency fall below some 20% in the best case, but there is a sharp falling-off at high p_T , as expected. The realistic contours are shown in the panel on the lower right, marked ‘Double b -tag with $\eta_b \neq 1$, and here we have a rather modest region even if we demand an efficiency of 10%, with only a small region revealing an efficiency of more than 15%.

In view of the efficiency plots presented in Figure 1 and discussed above, we suggest that a single b -tag may be a more efficient way of identifying Higgs jets than the double b -tag. Though our analysis will take both the cases into account, it will be seen that the single b -tag is better for the earlier runs of the LHC, while the double b -tag will serve to clinch the discovery – if made – in the later higher luminosity runs of the same machine.

A final comment is in order before we end this section and go on to our specific results. The analysis in this section, though showcased using the supersymmetric process in Equation (14), is really quite model-independent and the efficiency plots in Figure 1 are completely general, independent of the processes that produce the light Higgs boson h_1^0 . Our analysis can, therefore, be extended not only to light Higgs bosons, but to any object of comparable mass decaying to a pair of jets. This includes the W^\pm and Z^0 bosons, identifiable by their known masses, but also many exotics in some of the wide range of models which predict new physics.

4 Bump Hunting in Boosted Jets : CPX Scenario

Having set up the mechanism to identify boosted Higgs jets, we now apply this to the model of interest, viz., the CP-violating MSSM. There are several mechanisms by which the Higgs bosons h_i^0 ($i = 1, 2, 3$) can be produced in this model. We list some of the parton-level processes below.

- Gluon fusion: $g + g \rightarrow h_i^0$, which is the major production process in the SM. Here, however, the produced h_i^0 will have very small p_T .
- Vector boson fusion: $V + V \rightarrow h_i^0$, where $V = W^\pm, Z^0$, another SM process, where the

h_i^0 are produced in association with two highly forward jets.

- Higgstrahlung: $q + \bar{q}(\bar{q}') \rightarrow V^* \rightarrow V + h_i^0$, where $V = W^\pm, Z^0$, which is suppressed compared to the previous two, but produces h_i^0 with larger p_T .
- Associated production with top quarks: $p + p \rightarrow t + \bar{t} + h_i^0$, which also has a small cross section, but produces h_i^0 with large p_T .
- Associated production with gaugino states: $p + p \rightarrow \tilde{\chi}_{1,2}^\pm + \tilde{\chi}_{1,2}^\mp + h_i^0$ or $\tilde{\chi}_{1,2,3,4}^0 + \tilde{\chi}_{1,2,3,4}^0 + h_i^0$ or $\tilde{\chi}_{1,2}^\pm + \tilde{\chi}_{1,2,3,4}^0 + h_i^0$, which occur only in SUSY models.
- Chargino decay: $\tilde{\chi}_2^\pm \rightarrow \tilde{\chi}_1^\pm + h_i^0$ where the charginos are produced directly or in cascade decays of squarks/gluinos.
- Neutralino decay: $\tilde{\chi}_{2,3,4}^\pm \rightarrow \tilde{\chi}_1^\pm + h_i^0$ where the neutralinos are produced directly or in cascade decays of squarks/gluinos.
- Stop and sbottom decay: $\tilde{t}_2 \rightarrow \tilde{t}_1 + h_i^0$ and $\tilde{b}_2 \rightarrow \tilde{b}_1 + h_i^0$, where the heavier stop or sbottom can be either produced directly or arise as a product of gluino decay.
- Associated production with stop states: $p + p \rightarrow \tilde{t}_{1,2} + \tilde{t}_{1,2}^* + h_i^0$, which is similar to the associated production with top quarks.

The above list is illustrative, but not exhaustive, for there can be several stages in SUSY cascade decays where the h_i^0 can be produced. All these processes are, however, taken care of in our numerical simulation using PYTHIA.

Obviously, with so many contributing processes the LHC will produce large numbers of the h_i^0 as the run progresses. The question which interests us, however, is whether these produced h_i^0 's will be detectable using the tagging algorithm described in the previous section. For this, we have seen that the crucial kinematic determinant is the transverse momentum p_T . It is important, therefore, to have a clear picture of the p_T distribution of the three Higgs scalars h_i^0 . Unfortunately, this distribution is very sensitive to the masses of the h_i^0 and the mass-splitting between the different chargino and neutralino states, i.e. on the exact choice of model parameters. Thus, it is very difficult to make very general statements about the nature of these p_T distributions. Instead, we find it expedient to focus on the four benchmark points described in Table 1. Since these are chosen to cover various aspects of the CP-violating MSSM parameter space and guarantee the existence of light Higgs states, we can expect the p_T distributions of the h_i^0 at these points to carry information about the strengths and weaknesses of the Higgs-tagging algorithm.

Process	BP-1	BP-2	BP-3	BP-4
$\tilde{\chi}_2^0 \rightarrow \tilde{\chi}_1^0 + h_1^0$	99.6	98.8	10.4	98.4
$\tilde{\chi}_2^0 \rightarrow \tilde{\chi}_1^0 + h_2^0$	–	–	71.2	–
$\tilde{\chi}_2^0 \rightarrow \tilde{\chi}_1^0 + h_3^0$	–	–	18.0	–
$h_3^0 \rightarrow h_1^0 + h_1^0$	84.1	–	–	–
$h_2^0 \rightarrow h_1^0 + h_1^0$	51.9	–	–	–
$h_3^0 \rightarrow b + \bar{b}$	14.3	90.4	90.4	90.2
$h_2^0 \rightarrow b + \bar{b}$	43.7	90.7	90.7	90.5
$h_1^0 \rightarrow b + \bar{b}$	92.0	91.5	91.4	91.2
$\tilde{t}_2 \rightarrow \tilde{t}_1 + h_1^0$	0.23	0.02	0.01	0.06
$\tilde{t}_2 \rightarrow \tilde{t}_1 + h_2^0$	29.2	31.2	26.9	14.7
$\tilde{t}_2 \rightarrow \tilde{t}_1 + h_3^0$	26.9	19.2	24.8	42.0

Table 2: Some important branching ratios (per cent) for the four benchmark points of Table 1 in Section 2. Blank entries indicate that the corresponding decay is kinematically disallowed. Note that the h_1^0 always decay predominantly into $b\bar{b}$ pairs.

At the LHC, the production cross-section of the Higgs bosons depends not only on their masses, but also on their couplings and on the branching ratios of heavier particles to final states involving these Higgs particles. As there are many processes, this is not easy to predict or to explain. Some information about the principal production modes can be gleaned from a study of the branching ratios of gauginos to the Higgs states and the branching ratios of the latter to $b\bar{b}$ states. Some of these are listed in Table 2. From the table, it is obvious that the h_1^0 can arise from the decay of heavy gaugino as well as Higgs states, and that it always decays dominantly to $b\bar{b}$ pairs – as we have implicitly assumed in setting up the Higgs-tagging algorithm. The results shown in Table 2 also indicate that the benchmark point BP-3 will have qualitatively different features from the others, as we have already noted.

In Figure 2, we generate the p_T distributions for the three Higgs states. Black, red and blue histograms correspond, respectively, to the h_1^0 , h_2^0 and h_3^0 states for each of the four benchmark points on the corresponding panel in Figure 2, as marked. Since these plots are generated for a theoretical understanding of the Higgs-tagging algorithm, none of the standard kinematic cuts used in SUSY searches have been applied. These plots immediately tell us that for BP-1, BP-2 and BP-4, the lightest h_1^0 is the most produced of the three states, whereas for the BP-3, it is the heavier h_2^0 which is produced most copiously.

We are now in a position to correlate the p_T distributions of Figure 2 with the efficiency plots of Figure 1. Let us first consider the panel marked BP-1. In this case, the masses of the Higgs states are approximately 50, 100 and 130 GeV respectively. If we consider the panel marked ‘Single b -tag with $\eta_b \neq 1$ ’ in Figure 1, we note that for the lightest state, we

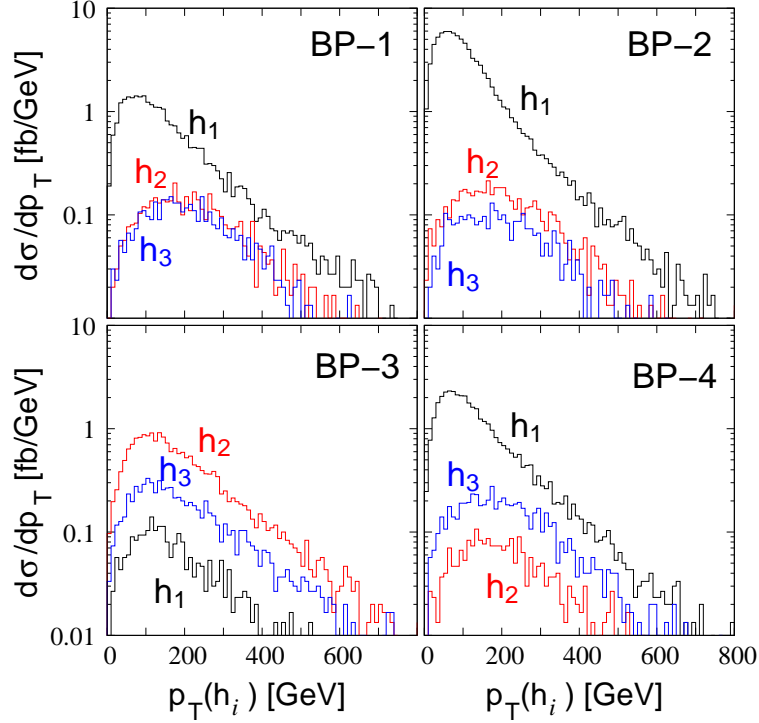


Figure 2: Distributions in transverse momentum $p_T(h_i)$ for the three Higgs bosons h_i^0 ($i = 1, 2, 3$) at the 14-TeV LHC. Black, red and blue histograms correspond, respectively, to the h_1^0 , h_2^0 and h_3^0 states (as marked). The four panels in this plot are marked BP-1, BP-2, BP-3 and BP-4, corresponding to the parameter choices of Table 1. No kinematic cuts were applied to generate these distributions.

can obtain a tagging efficiency above 30% for the p_T range $200 - 400$ GeV. This is not the peak region of the p_T distribution shown in Figure 2, but just to the right of it. It follows that the tagging algorithm will miss a fairly large fraction of the Higgs bosons, though it will still be able to capture a significant number. We shall see presently that this is enough to identify the Higgs state. For the moment, we focus on the other states, where we have to go to $p_T > 400$ GeV to obtain any useful efficiency. However, for such large values of p_T , the production cross section for these states is at least an order of magnitude smaller than that of the h_1^0 in the region where it can be tagged with reasonable efficiency. Thus, we should not expect any useful signal from the production of these states, i.e. they will remain invisible to our study. For such states, we will have to turn to the rare $\gamma\gamma$ decay mode, which is a much more difficult study and beyond the scope of this work.

For the other benchmark points, we can carry out a similar analysis based on a combination of Figures 1 and 2. Despite the variation in parameters, the conclusions for BP-2 and BP-4 are very similar to that of BP-1, and hence are not detailed here. For BP-3, however, the situation is somewhat different. As in the case of BP-1, reasonable efficiencies for the heavy

h_2^0 state (~ 113 GeV) take us into the high- p_T regime, where we pick up only the tail of the p_T distribution, whereas the lightest h_1^0 state (~ 72 GeV) can be tagged with better efficiency in the range where it is produced more copiously. However, the overall production of the h_2^0 is so much larger than that of the h_1^0 that we should expect the final cross section for the h_2^0 to be at least comparable with that of the h_1^0 . We should not expect much from the h_3^0 , which is neither light enough to avail of the higher efficiencies, nor is produced in enough numbers to offset that disadvantage.

If we now pass from the ‘Single b -tag with $\eta_b \neq 1$ ’ to the ‘Double b -tag with $\eta_b \neq 1$ ’, we shall obtain very similar results, except that the efficiencies will drop by a factor of 3 or more. Hence discovery through this mode will require the collection of more data than the previous case. However, as mentioned before, this should be treated as secondary, clinching evidence once we have a definite signal in the ‘Single b -tag with $\eta_b \neq 1$ ’ data sample.

The results of Figures 1 and 2 and the arguments presented above make a reasonable case for using the tagging algorithm of Section 3 as a tool in a search for light Higgs bosons in the CP-violating MSSM. However, such a study now requires to be carried out with a full PYTHIA simulation including all relevant processes and with jet identification through the FASTJET package, as explained in Section 3 for a toy model. We have carried out this study for the four benchmark points as above, after generating the SUSY mass spectrum and couplings using CPSUPERH as incorporated in the CALCHEP package [57]. Parton density functions of the CTEQ5L set [58] have been used and the factorisation scale is set to the parton-level energy. The final states of interest either have multijets and large missing p_T (\cancel{p}_T) or one hard lepton, multijets and large \cancel{p}_T . After generating each event, we have applied the following kinematic cuts, which are more-or-less in line with those applied in standard SUSY searches by the CMS Collaboration [59]. These are listed below.

1. We select events with jets (J) having transverse momentum $p_T^J > 30$ GeV and pseudorapidity $|\eta_J| < 3$. The identified jets will be labelled J_1, J_2, \dots in order of decreasing p_T^J .
2. The events must have⁷ missing transverse momentum satisfying $\cancel{p}_T > 300$ GeV. To calculate this, we take into account all jets with $p_T^J > 20$ GeV and pseudorapidity $|\eta_J| < 4.5$ and all leptons with $p_T^\ell > 10$ GeV and pseudorapidity $|\eta_\ell| < 2.5$.
3. The leading (maximum p_T) jet must have pseudorapidity $|\eta_{J_1}| < 1.7$.

⁷Here we deviate a little from the CMS analysis, which has $\cancel{p}_T > 200$ GeV.

4. The two leading jets must have $p_T^{J_1} > 180$ GeV and $p_T^{J_2} > 110$ GeV.
5. We calculate an effective mass $M_{\text{eff}} = p_T^{J_2} + p_T^{J_3} + p_T^{J_4} + \cancel{p}_T$ and impose the condition $M_{\text{eff}} > 500$ GeV. Naturally, $p_T^{J_4}$ is added only if the corresponding jet exists.
6. The angular separation between the two leading jets and the \cancel{p}_T are calculated as $R_1 = \sqrt{(\pi - \delta\varphi_1)^2 + \delta\varphi_2^2}$ and $R_2 = \sqrt{\delta\varphi_1^2 + (\pi - \delta\varphi_2)^2}$, where $\delta\varphi_1 = |\phi_{j_1} - \phi_{\cancel{p}_T}|$ and $\delta\varphi_2 = |\phi_{j_2} - \phi_{\cancel{p}_T}|$. On these, we impose the conditions that $R_{1,2} > 0.5$.
7. The azimuthal angular separation between all jets and the \cancel{p}_T must satisfy the criterion $\delta\varphi_1 = |\phi_j - \phi_{\cancel{p}_T}| > 0.3$.
8. The azimuthal angular separation between the next-to-leading jet and the \cancel{p}_T must satisfy the criterion $\delta\varphi_2 = |\phi_{j_2} - \phi_{\cancel{p}_T}| > 0.35$.
9. We impose a lepton veto, i.e. the event should not contain any isolated lepton with $p_T^\ell > 20$ GeV and $|\eta_\ell| < 2.5$. The isolation criteria imposed on each lepton are (a) that the angular separation $\Delta R_{\ell J}$ between the lepton and every jet should not be less than 0.4 and (b) that the sum of the scalar p_T of all stable visible particles within a cone of radius $\Delta R = 0.2$ around the lepton should not exceed 10 GeV.

	BP-1	BP-2	BP-3	BP-4	$t\bar{t}$
Sample	114 000	111 090	108 720	109 170	11 070 000
Cut 1	103 880	101 968	80 624	99 910	7 208 031
Cut 2	11 161	11 539	13 778	11 012	19 360
Cut 3	10 489	10 861	12 726	10 410	17 156
Cut 4	9 759	10 041	10 942	9 695	12 165
Cut 5	9 745	10 025	10 896	9 684	11 997
Cut 6	8 237	8 517	9 451	8 225	7 372
Cut 7	5 220	5 452	6 335	5 211	4 697
Cut 8	5 199	5 431	6 317	5 193	4 679
Cut 9	3 436	3 814	5 089	3 501	1 880

Table 3: Kinematic cut flow table for a luminosity of 30 fb^{-1} at each of the benchmark points BP-1 to BP-4. The cuts are numbered as in the text. Note the drastic effect of Cut 2, which requires $\cancel{p}_T > 300$ GeV. The efficacy of these cuts in removing the enormous $t\bar{t}$ background is immediately obvious.

It is interesting to see how the raw signal plotted in Figure 2 is affected by the different cuts enumerated above. The total SUSY cross sections are rather large, being at the level of 3.8 pb, 3.7 pb, 3.6 pb and 3.6 pb for the benchmark points BP-1, BP-2, BP-3 and BP-4 respectively, but are dwarfed by the $t\bar{t}$ cross section which is 369 pb at the lowest order. The effects of the different cuts on the cross section are displayed in Table 3, where we assume

an integrated luminosity of 30 fb^{-1} . The numbering 1–9 of the cuts is exactly as in the text above. The crucial role of the Cut 2 (on p_T) is obvious, and may be taken as a justification of the choice of a stronger cut than that of the CMS collaboration. It is also interesting to note that it is the lepton veto which finally reduces the $t\bar{t}$ background to a tractable value without affecting the signal events quite as strongly.

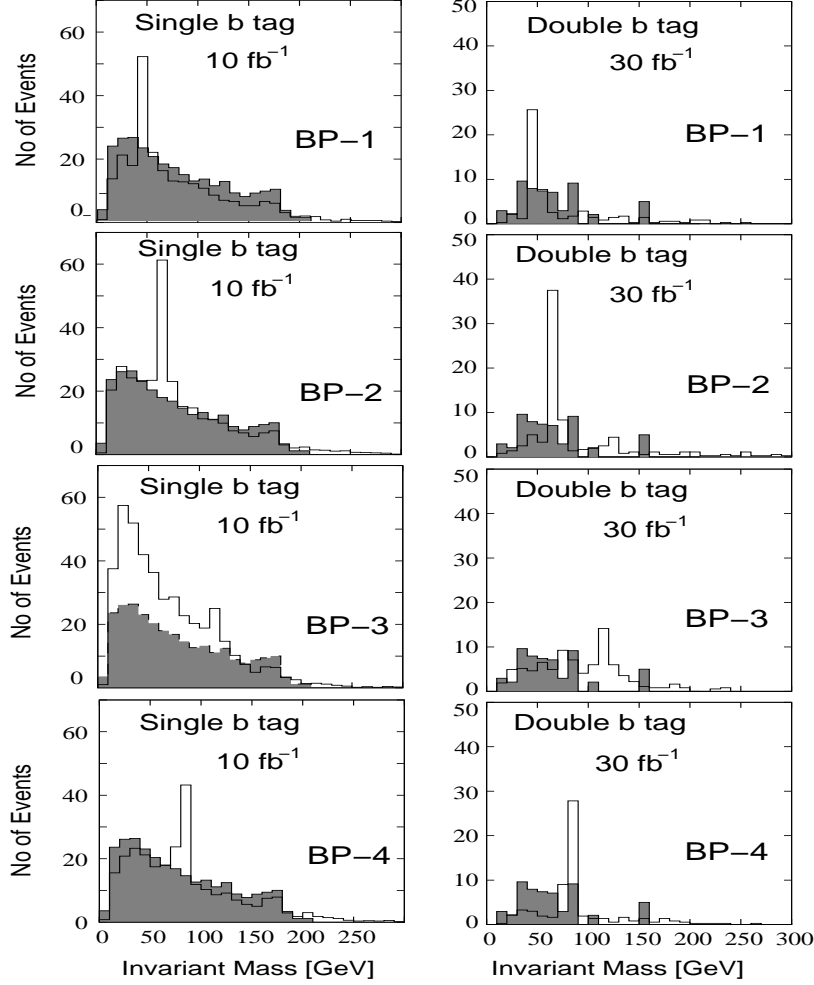


Figure 3: Bin-wise invariant mass distribution of the leading jet with single (double) b -tags in 10 (30) fb^{-1} of data at the 14 TeV LHC. The shaded histogram represents the $t\bar{t}$ background. Note the clear resonances corresponding to the lightest Higgs boson h_1^0 for the benchmark points BP-1, BP-2 and BP-4 (marked on the respective panels). For BP-3 and a single b -tag, we find a modest resonance corresponding to the h_2^0 , while, for a double b -tag, there is only a tiny bump corresponding to the h_2^0 .

The results of our numerical study are presented in Figure 3, where we have plotted distributions in the invariant mass of the leading jet (identified as a Higgs jet) by the algorithm of Section 3. In every panel, the unshaded histograms represent the signal and the shaded histograms represent the $t\bar{t}$ background, which is the dominant SM background. Each row of

panels corresponds to one of the benchmark points of Table 1, as marked on the corresponding panels. The left (right) column corresponds to studies with a single (double) b -tag. To compensate for the lower efficiencies in the latter case, we use a higher luminosity of 30 fb^{-1} instead of the 10 fb^{-1} used for the former.

The results for BP-1, BP-2 and BP-4 are very similar: in each case with a single b -tag we get a clear peak corresponding to the h_1^0 resonance. Taking the $t\bar{t}$ background alone, and the single bin of interest, this would be a deviation from the SM prediction at the level of around 10σ in each case — which means that a discovery can be claimed in the very early stages of the 14 TeV LHC run. A similar statement can be made for the double b -tags with our higher luminosity assumption. For the benchmark point BP-3, with a single b -tag, a large and broad excess region can be found, with a small peak corresponding to h_2^0 . On the other hand, for a double b -tag, the same benchmark point reveals rather disappointing results, with the signal hardly distinguishable from fluctuations in the $t\bar{t}$ histogram.

On the whole, therefore, we can conclude that prospects for detecting the lightest Higgs boson of the CP-violating MSSM by tagging ‘fat’ jets are rather bright. The single b -tag alone gives very clear resonant peaks in the invariant mass distribution of the ‘fat’ jets, and, if the parameters are favourable, one can expect confirming signals using the double b -tag method as well. It is only fair, however, to mention that our estimation of the background is somewhat crude and is limited to the $t\bar{t}$ signal at the leading order (LO). We know, of course, that addition of next-to-leading order (NLO) corrections to the $t\bar{t}$ cross section can increase the cross section by a factor of 2 or more. In that case, the background indicated by the shaded histogram in the figure will grow by a corresponding factor and the resonant peaks of the signal may not stand so tall above background as they appear in Figure 3. However, this is no reason to be disheartened, for (a) the Higgs boson production modes will also receive comparable enhancements when NLO corrections are added, and (b) what will be observed will be the sum of signal and background events, and if this is compared with the random fluctuation in the background, the single b -tag signal with 10 fb^{-1} of data will still be at a level of more than 5σ , which is all that we require for a discovery.

Before we end this section it is appropriate to comment on other backgrounds, apart from those due to $t\bar{t}$ production. The standard cuts devised for SUSY searches and applied to this signal will effectively remove backgrounds arising from the production of electroweak bosons, as may be guessed from the complete absence of peaks in the vicinity of M_W and M_Z in Figure 3 — unless, indeed, a light Higgs boson happens to lie just there. However,

there will be a pure QCD background, which, despite drastic reduction by the same cuts and a very small mistagging probability, may still be expected to contribute something to the background because the initial cross section is many orders of magnitude larger than the signal. In this work, we have not attempted any detailed estimate of the QCD background or the mistagging probability, but a rough estimate based on the results of Ref. [59] shows that the QCD background will not be more than a few femtobarns, whereas our signal, even after application of all cuts is around 100 fb. Another possibility is that of backgrounds arising from the production and decay of supersymmetric particles, which we have not estimated, but surely forms some fraction of what we have identified as the signal. Once again, we have not attempted a detailed study of these, but we can guess from the fairly tall and sharp resonances that we seem to be predicting for the light Higgs states, that these backgrounds will not really prove a difficulty when the experimental data are available.

5 Beyond the CPX Scenario

We have seen in the previous section that one can use jet substructure analyses very effectively to probe hitherto-invisible Higgs bosons in the CPX scenario, as exemplified through our choice of four benchmark points. However, one can now ask whether a similar analysis can be used in a more general context than the CPX scenario, which itself is a benchmark created to showcase a ‘blind spot’ in previous collider searches for the CP-violating MSSM. A detailed answer of this question would require a detailed scan of the parameter space to determine the exact extent of this collider-invisible region – a lengthy and tedious business, given the large number of parameters which come into play when we allow the MSSM to become CP-violating. However, a partial answer, at least, can be sought by again picking up a couple of benchmark points, BP-5 and BP-6, which do not conform to the CPX parametrisation, but are nevertheless part of the ‘blind spot’, i.e. invisible to collider searches using conventional strategies.

BP	M_1	M_2	$\tan\beta$	$M(H^\pm)$	μ	Φ_{CP}	$M(h_1^0)$	$M(h_2^0)$	$M(h_3^0)$	$M(\tilde{\chi}_1^0)$	$M(\tilde{\chi}_1^\pm)$
5	100	200	8	130	2400	$\pi/2$	37.2	110.4	132.5	99.8	199.1
6	150	400	11	135	2000	$3\pi/4$	56.8	117.3	127.7	149.8	398.7

Table 4: Benchmark points lying outside the CPX scenario, but within the ‘blind spot’ for collider searches. Free parameters not explicitly given in the table are taken identical with those in the CPX scenario of the previous section. All masses are in units of GeV.

As before, we exhibit our choice of benchmark points in Table 4, where, in addition to the free parameters, we display part of the mass spectrum. The choice of BP-5 is dictated by a

desire to make the lightest Higgs boson h_1^0 as light as possible – and here it can be as low as about 37 GeV. The mass spectrum for BP-6 is rather similar to that of BP-3. The crucial difference here lies in the branching ratios exhibited in Table 5, where we note that the $\tilde{\chi}_2^0$ can decay with a reasonable branching ratio into the $\tilde{\chi}_1^0$ plus any one of the three Higgs states h_1^0 , h_2^0 and h_3^0 . In this case, we could perhaps have comparable numbers of all the three Higgs states produced and look for all of them together using our tagging algorithm.

Process	BP-5	BP-6
$\tilde{\chi}_2^0 \rightarrow \tilde{\chi}_1^0 + h_1^0$	99.7	61.9
$\tilde{\chi}_2^0 \rightarrow \tilde{\chi}_1^0 + h_2^0$	–	23.8
$\tilde{\chi}_2^0 \rightarrow \tilde{\chi}_1^0 + h_3^0$	–	13.9
$h_3^0 \rightarrow h_1^0 + h_1^0$	72.5	21.2
$h_2^0 \rightarrow h_1^0 + h_1^0$	88.4	30.5
$h_3^0 \rightarrow b + \bar{b}$	23.5	71.3
$h_2^0 \rightarrow b + \bar{b}$	10.5	63.0
$h_1^0 \rightarrow b + \bar{b}$	92.4	91.7
$\tilde{t}_2 \rightarrow \tilde{t}_1 + h_1^0$	0.09	0.06
$\tilde{t}_2 \rightarrow \tilde{t}_1 + h_2^0$	20.2	17.5
$\tilde{t}_2 \rightarrow \tilde{t}_1 + h_3^0$	36.8	34.8

Table 5: Some important branching ratios (per cent) for the four benchmark points of Table 4. Blank entries indicate that the corresponding decay is kinematically disallowed.

Having made this choice, we once again start by investigating the p_T distribution of the Higgs states to get a crude impression of how effective the Higgs tagging algorithm can be. Our results are presented in Figure 4, which resembles Figure 2 closely, except that the panels correspond to BP-5 and BP-6 rather than BP-1 to BP-4. The histograms in black, red and blue correspond to the h_1^0 , h_2^0 and h_3^0 states respectively. The left (right) panel corresponds to BP-5 (BP-6) as marked. The qualitative features of these two plots are very different: for BP-5, production of h_1^0 bosons is overwhelmingly dominant over production of h_2^0 and h_3^0 , whereas the numbers are more comparable for BP-6. The reason for this lies less in the kinematics than in the dominant branching ratio of $\tilde{\chi}_2^0$ decays to the h_1^0 in the BP-5 case, as exhibited in Table 5 below.

Once again, it is interesting to compare Figure 4 with the efficiency plots in Figure 1. Concentrating on BP-5 for the moment, let us note that for a h_1^0 mass as low as 37 GeV, reasonable Higgs-tagging efficiencies can be obtained in the p_T range 150 – 400 GeV, which allows us to include a little more of the peak region of the p_T histogram than was the case for, say, BP-1. Thus we may expect a somewhat taller resonance for the h_1^0 in this case than was

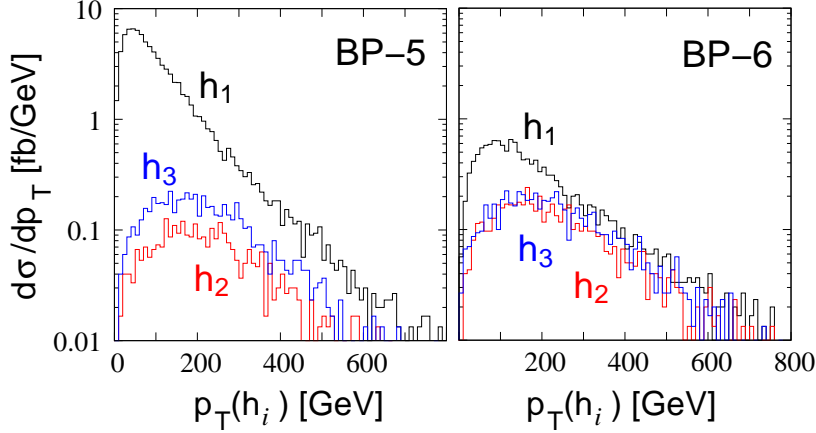


Figure 4: Distributions in transverse momentum $p_T(h_i)$ for the three Higgs bosons h_i^0 ($i = 1, 2, 3$) at the 14-TeV LHC. Black, red and blue histograms correspond, respectively, to the h_1^0 , h_2^0 and h_3^0 states. The panels in this plot are marked BP-5 and BP-6, corresponding to the parameter choices of Table 4. No kinematic cuts were applied to generate these distributions.

found for BP-1 and similar cases. In this case, the number of h_2^0 and h_3^0 produced is too small to expect any signals over the substantial $t\bar{t}$ background. If we carry out a similar analysis for the case of BP-6, we will find that all three Higgs bosons have comparable chances of producing a resonance in tagged ‘fat’ jets, though even here the h_1^0 will have a slight edge over the others due to its lighter mass and greater tagging efficiency.

The above arguments enable us to make some crude guesses about the possible results, but it is necessary to carry out the full Monte Carlo simulation as in the previous section before we can say anything more definitive. In order to do this, we use the same machinery as described in the previous section, with the identical set of cuts and efficiency assumptions. The results of our numerical simulations are displayed in Figure 5, where, as in Figure 3, we plot distributions in the invariant mass of the leading jet (identified as a Higgs jet by the algorithm of Section 3). The upper row of panels corresponds to the benchmark point BP-5 of Table 4, as marked on the panels, while the lower row corresponds to the benchmark point BP-6. As before, the left column corresponds to studies with a single b -tag with 10 fb^{-1} , while the right column presents the results with a double b -tag and 30 fb^{-1} of data. As in Figure 3, the unshaded histograms represent the signal while the shaded histograms represent the $t\bar{t}$ background.

These results are more-or-less as expected from the previous discussion, where we took the p_T distribution and the efficiency plot of Figure 1 jointly into consideration. For the benchmark point BP-5, with a 37 GeV Higgs state, we get tall resonances in the ‘fat’ jet invariant mass. Here the single b -tag method would produce a signal even for 1 fb^{-1} of data. Of all the

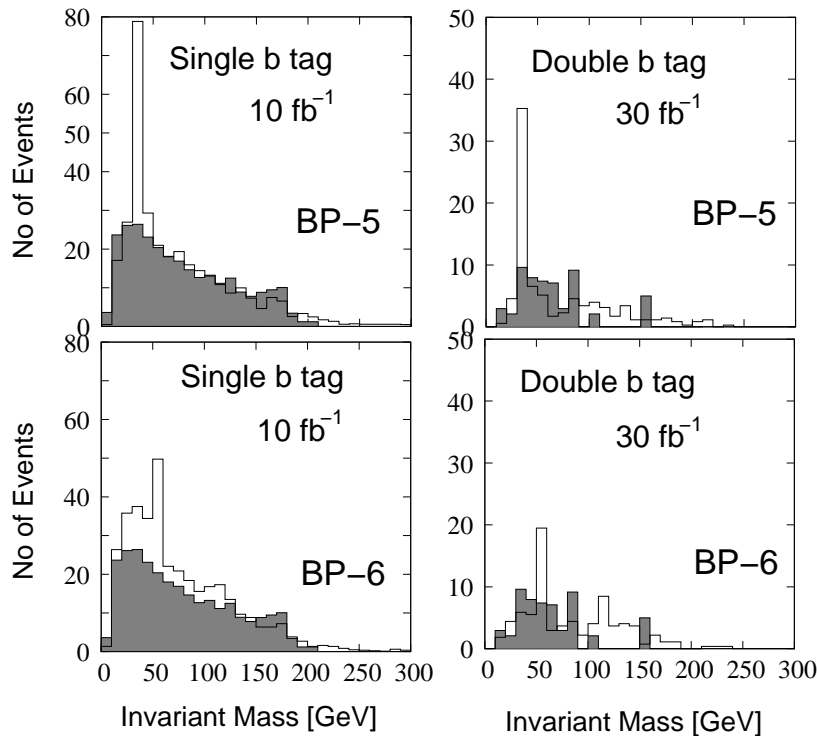


Figure 5: Bin-wise invariant mass distribution of the leading jet with single (double) b -tags in 10 (30) fb^{-1} of data at the 14-TeV LHC for the benchmark points BP-5 and BP-6 (marked on the respective panels). Note the clear h_1^0 resonance for BP-5 with both single and double b -tags. For BP-6 we find small resonances corresponding to the h_1^0 and h_2^0 . The shaded histogram represents the $t\bar{t}$ background.

benchmark points considered, this is definitely the best signal we get, and thus, if we are lucky, even the first few months of running of the LHC at 14 TeV would throw up a light Higgs discovery. On the other hand, if we consider the other benchmark point BP-6, the signal is much weaker, but it seems just possible to detect the h_1^0 as well as an h_2^0 state. The evidence for the latter, as evinced in Figure 5, is not very strong, but would certainly improve as more data are collected. Discovery of a second Higgs boson would go a long way towards establishing a CP-violating Higgs sector, and more generally, a BSM Higgs sector.

6 Summary and Outlook

In this article, we have presented arguments to show that the existence of light Higgs scalars with masses below 100 GeV is by no means ruled out by existing data, except within the very restrictive assumptions made in the SM and in the MSSM without CP violation. As an example of a model where relaxation of these assumptions permits the existence of light Higgs bosons, we have chosen the CP-violating version of the MSSM, and argued that this is by no means an exotic model, but a very natural version of a supersymmetric model. In this

model, we have picked on a set of parameters known as the CPX scenario, which is known to lie in a ‘blind spot’ of all collider searches till the present – including the LEP-1 and LEP-2, the Tevatron and the just-concluded runs of the LHC. To keep the discussion focussed, we have chosen four benchmark points in the CP-violating MSSM, all of which lie within the CPX scenario, and verified that these all correspond to light Higgs bosons which would be completely invisible to all the above-mentioned collider searches. Of course, except for our specific choice of the benchmark points, all of this is simply a reiteration of facts or results available in the literature.

The novel feature of our work is the suggestion that the ‘blind spot’ of previous collider searches may actually be explored at the LHC using recently-developed Higgs-tagging techniques using jet substructure. Once again, such techniques have been described in the literature earlier, and even applied to study Higgs bosons in the CP-conserving MSSM, though with somewhat modest results [40]. In our work, we simply follow the original algorithm for Higgs tagging, with some small modifications to the case of interest, as described in Section 3. The results of our study are showcased in Figure 1, where the efficiency contours in the plane of Higgs p_T and Higgs mass clearly show that the method is much more efficient for light Higgs bosons than for Higgs bosons in the range permitted by the SM and CP-conserving MSSM. When we apply it to the benchmark points chosen within the CPX scenario, we find that clearly-identifiable resonances corresponding to the lightest Higgs boson appear in the invariant mass distribution of all jets which pass through the Higgs tagging algorithm. For some points, one can even discern hints of a second Higgs boson. These encouraging results appear to be found whether we tag one or both of the b sub-jets resulting from the Higgs decays.

Emboldened by our findings, we have extended our study beyond the CPX scenario to other parts of the ‘blind’ region, where we have selected another two benchmark points, with distinct features in the mass spectra and branching ratios. Here again, we have found very clear resonances, indicating that the same technique can be a powerful probe of a large part, if not all, of the hitherto ‘blind spot’ of collider searches in the CP-violating MSSM, over and above the CPX region.

The purpose of this work was to establish that the Higgs-tagging algorithm can be used effectively to probe the ‘blind spot’ of the CP-violating MSSM, and we believe that has been adequately established by our getting positive results at all the six benchmark points chosen. A more detailed mapping of the ‘blind spot’ is in progress [47]. In fact, we have

already remarked that this method can also probe other models with light Higgs bosons, for the Higgs-tagging algorithm works so long as these Higgs bosons are boosted and decay to $b\bar{b}$ pairs.

Eventually, we hope that this powerful technique will be taken up by the experimental collaborations and applied to real data, instead of Monte Carlo simulations as was done in this exploratory study. The most exciting possibility, of course, would be if experimental searches could use this technique to actually find a light Higgs resonance, which has been missed in all collider searches so far. If not, we will have to settle, as usual, for a more constrained parameter space for the model in question. In either case, the present technique could be the key to accessing the region which previous searches could not, and that alone represents a modest degree of progress.

Acknowledgement

The work of BB is supported by World Premier International Research Center Initiative (WPI Initiative), MEXT, Japan. DKG acknowledges partial support from the Department of Science and Technology, India, under the grant SR/S2/HEP-12/2006. BB, AC and DKG are grateful to, respectively, the IACS (Kolkata, India), the TIFR (Mumbai, India) and the KIAS (Seoul, Korea), for hospitality while part of this work was being done. AC thanks Subir Sarkar for programming help and guidance, while SR acknowledges useful discussions with Tuhin S. Roy.

References

- [1] P.W.Higgs, Phys. Lett. **12**, 132 (1964); Phys. Rev. Lett. **13**, 506 (1964); F.Englert and R.Brout, Phys. Rev. Lett. **13**, 321 (1964); G.Guralnik, C.Hagen and T.Kibble, Phys. Rev. Lett. **13**, 585 (1964).
- [2] Y.Nambu, Phys. Rev. Lett. **4**, 380 (1960); Y.Nambu and G. Jona-Lasinio, Phys. Rev. **122**, 345 (1961); *ibid.* Phys. Rev. **124**, 246 (1961); J. Goldstone, Nuov. Cim. **19**,154 (1961); J. Goldstone, A. Salam and S. Weinberg, Phys. Rev. **127**, 965 (1962).
- [3] For reviews on the Higgs sector, see: J. Gunion, H. Haber, G. Kane and S. Dawson, *The Higgs Hunter's Guide*, (Addison–Wesley, Reading 1990); A. Djouadi, Phys. Rept. **457**, 1 (2008).
- [4] The LEP collaborations and the LEP electroweak working group, hep-ex/0612034; <http://lepewwg.web.cern.ch/LEPEWWG/> .
- [5] G. Aad *et al.* [ATLAS Collaboration], Phys. Lett. B **716**, 1 (2012) [arXiv:1207.7214 [hep-ex]]; S. Chatrchyan *et al.* (CMS Collaboration), CERN preprint CERN-PH-EP/2012-220, arXiv:1207.7235 (July 2012); TEVNPH Working Group (for the CDF, D0 Collaborations), Fermilab preprint FERMILAB-CONF-12-318-E, arXiv:arXiv:1207.0449 [hep-ex] (2012).
- [6] P.P. Giardino *et al.*, CERN preprint CERN-PH-TH/2012-208, arXiv:1207.1347 (2012); T. Plehn and M. Rauch, arXiv:1207.6108 (2012).
- [7] LEP working group for Higgs searches, R.Barate *et al.*, Phys. Lett. **B565**,61 (2003).
- [8] LEP Higgs Working Group, LHWG Note 2005-01, presented at the Lepton Photon Symposium (2005).
- [9] J.F. Gunion, B. Grzadkowski, H.E. Haber and J. Kalinowski, Phys. Rev. Lett. **79**, 982 (1997).
- [10] For a review see M.Dine and A.Kusenko, Rev. Mod. Phys. **76**, 1 (2003), arXiv:hep-ph/0303065.
- [11] P.Nath, Phys. Rev. Lett. **66**, 2565 (1991); Y.Kizukuri and N.Oshino, Phys. Rev. **D46**, 3025 (1992); T.Ibrahim and P.Nath, Phys. Lett. **B418**, 98 (1998), arXiv:hep-ph/9707409; Phys. Rev. **D57**, 478 (1998), arXiv:hep-ph/9708456; *ibid.* **D58**, 019901(E) (1998); *ibid.* **D60**, 079903 (1999); *ibid.* **D60**, 119901 (1999); M.Brhlík, G.J.Good and G.L.Kane, Phys. Rev. **D59**, 115004 (1999), arXiv:hep-ph/9810457; A.Bartl *et al.*, Phys. Rev. **D60**, 073003 (1999), arXiv:hep-ph/9903402; D.Chang, W.-Y.Keung and A.Pilaftsis, Phys. Rev. Lett. **82**, 900 (1999), arXiv:hep-ph/9811202; S.Pokorski, J.Rosiek and C.A.Savoy, Nucl. Phys. **B570**, 81 (2000), arXiv:hep-ph/9906206; E.Accomando, R.Arnowitz and B.Dutta, Phys. Rev. **D61**, 115003 (2000), arXiv:hep-ph/9907446; S.Abel, S.Khalil and O.Lebedev, Nucl. Phys. **B606**, 151 (2001), arXiv:hep-ph/0103320; U.Chattopadhyay, T.Ibrahim and D.P.Roy, Phys. Rev. **D64**, 013004 (2001), arXiv:hep-ph/0012337; D.A.Demir, M.Pospelov and A.Ritz, Phys. Rev. **D67**, 015007 (2003), arXiv:hep-ph/0208257.

- [12] A. Pilaftsis, Nucl. Phys. **B644**, 263 (2002), arXiv:hep-ph/0207277.
- [13] T. Falk, K.A. Olive, M. Pospelov and R. Roiban, Nucl. Phys. **B560**, 3 (1999), arXiv:hep-ph/9904393.
- [14] T. Ibrahim *et al.* and M. Brhlik, *et al.* in Ref. [11].
- [15] Y. Kizukuri, N. Oshimo in Ref. [11].
- [16] S. Abel and J.-M. Frere, Phys. Rev. **D55**, 1623 (1997).
- [17] D. Chang *et al.* in Ref. [11].
- [18] A. Dedes and S. Moretti, Phys. Rev. Lett. **84**, 22 (2000), arXiv:hep-ph/9908516, Nucl. Phys. **B576**, 29 (2000), arXiv:hep-ph/990941; S.-Y. Choi, K. Hagiwara and J.S. Lee, Phys. Rev. **D64**, 032004 (2001), arXiv:hep-ph/0103294, Phys. Lett. **B529**, 212 (2002), arXiv:hep-ph/0110138; A.G. Akeroyd and A. Arhrib, Phys. Rev. **D64**, 095018 (2001), arXiv:hep-ph/0107040; A. Arhrib, D.K. Ghosh and O.C.W. Kong, Phys. Lett. **B537**, 217 (2002) arXiv:hep-ph/0112039; S.Y. Choi, M. Drees, J.S. Lee and J. Song, Eur. Phys. J. **C25**, 307 (2002) arXiv:hep-ph/0204200; R.M. Godbole, S. Kraml, S.D. Rindani and R.K. Singh, Phys. Rev. **D74**, 095006 (2006); S. Moretti, S. Munir, P. Poulose, Phys. Lett. **B649**, 206 (2007); S. Hesselbach, S. Moretti, S. Munir and P. Poulose, Eur. Phys. J. **C54**, 129 (2008); F. Deppisch and O. Kittel, JHEP **0909**, 110 (2009) [Erratum-*ibid.* **1003**, 091 (2010)]; JHEP **1006**, 067 (2010); K.E. Williams, H. Rzehak and G. Weiglein, Eur. Phys. J. **C71**, 1669 (2011); O. Stal and G. Weiglein, arXiv:1108.0595 [hep-ph].
- [19] A. Pilaftsis, Phys. Rev. **D58**, 096010 (1998); Phys. Lett. **B435**, 88 (1998).
- [20] A. Pilaftsis and C.E.M. Wagner, Nucl. Phys. **B553**, 3 (1999).
- [21] D.A. Demir, Phys. Rev. D **D60**, 055006 (1999).
- [22] S.Y. Choi, M. Drees and J.S. Lee, Phys. Lett. **B481**, 57 (2000).
- [23] M. Carena, J.R. Ellis, A. Pilaftsis and C.E.M. Wagner, Phys. Lett. **B495**, 155, (2000); Nucl. Phys. **B586**, 92 (2000).
- [24] G.L. Kane and L.-T. Wang, Phys. Lett. **B488**, 383 (2000).
- [25] A. Sopczak for the LEP Higgs Working Group, presented at SUSY-2005, arXiv:hep-ph/0602136.
- [26] M. Carena, J.R. Ellis, S. Mrenna, A. Pilaftsis and C.E.M. Wagner, Nucl. Phys. **B659**, 145 (2003), arXiv:hep-ph/0211467.
- [27] G. Abbiendi *et al.* [OPAL Collaboration], Eur. Phys. J. **C37**, 49 (2004).
- [28] V. Buescher and K. Jakobs, Int. J. Mod. Phys. **A20**, 2523 (2005); arXiv:hep-ph/0504099.

- [29] M. Schumacher, talk at SUSY-04, arXiv: hep-ph/0410112.
- [30] E. Accomando *et.al.*, arXiv: hep-ph/0608079.
- [31] D.K. Ghosh, R.M. Godbole and D.P. Roy, Phys. Lett. **B628**, 131 (2005).
- [32] D.K. Ghosh, S. Moretti, Eur. Phys. J. **C42**, 341 (2005).
- [33] P. Bandyopadhyay, A. Datta, A. Datta and B. Mukhopadhyaya, Phys. Rev. **D78**, 015017 (2008); A.C. Fowler and G. Weiglein, JHEP **01**, 108 (2010); P. Draper, T. Liu, and C.E.M. Wagner, Phys. Rev. **D81**, 015014 (2010); P. Bandyopadhyay, JHEP **08**, 016 (2011); P. Bandyopadhyay and K. Huitu, arXiv:1106.5108 [hep-ph].
- [34] M.H. Seymour, Z. Phys. **C62**, 127 (1994).
- [35] J.M. Butterworth, J.R. Ellis and A.R. Raklev, JHEP **0705**, 033 (2007)
- [36] J.M. Butterworth, A.R. Davison, M. Rubin and G.P. Salam, Phys. Rev. Lett. **100**, 242001 (2008)
- [37] J. Thaler and L.T. Wang, JHEP **0807** (2008) 092
- [38] D.E. Kaplan *et al*, Phys. Rev. Lett. **101**, 142001 (2008)
- [39] A. Abdesselam *et al.*, Eur. Phys. J. **C71**, 1661 (2011); A. Altheimer *et al.*, arXiv:1201.0008 [hep-ph].
- [40] D. Ghosh, M. Guchait and D. Sengupta, TIFR preprint TIFR/TH/12-04 (2012), arXiv: 1202.4937 [hep-ph].
- [41] J.S. Lee *et al*, Comput. Phys. Commun. **180**, 312 (2009) arXiv:0712.2360 [hep-ph].
- [42] P. Bechtle *et al*, Comput. Phys. Commun. **181**, 138 (2010) arXiv:0811.4169 [hep-ph].
- [43] K. Agashe *et al*, Phys. Rev. **D77**, 015003 (2008); L.G. Almeida *et al*, Phys. Rev. **D79**, 074017 (2009) and *ibid.* **79**, 074012 (2009); D. Krohn, J. Shelton and L.T. Wang, JHEP **1007**, 041 (2010); B. Bhattacharjee, M. Guchait, S. Raychaudhuri and K. Sridhar, Phys. Rev. **D82**, 055006 (2010); T. Plehn, M. Spannowsky, M. Takeuchi and D. Zerwas, JHEP **1010**, 078 (2010); K. Rehermann and B. Tweedie, arXiv:1007.2221 [hep-ph]; P. Bandyopadhyay and B. Bhattacharjee, Phys. Rev. **D84**, 035020 (2011); T. Gregoire, E. Katz and V. Sanz, arXiv:1101.1294 [hep-ph]; T. Plehn, M. Spannowsky and M. Takeuchi, Phys. Rev. **D85**, 034029 (2012); J. Berger, M. Perelstein, M. Saelim and A. Spray, arXiv:1111.6594 [hep-ph].
- [44] CDF Collaboration, CDF note 10202 (2010).
- [45] J.S. Lee and S. Scopel, Phys. Rev. **D75**, 075001 (2007), hep-ph/0701221.
- [46] R. Aaij *et al* [LHCb Collaboration], Report No CERN-PH-EP-2012-072, LHCb-PAPER-2012-007 (2012), arXiv:1203.4493 [hep-ex].

- [47] B. Bhattacharjee, A. Chakraborty, D.K. Ghosh and S. Raychaudhuri (work in progress).
- [48] J. Thaler and K. Van Tilburg, JHEP **1103**, 015 (2011); Y. Cui, Z. Han and M.D. Schwartz, Phys. Rev. **D83**, 074023 (2011); Z. Han, arXiv:1112.3378 [hep-ph]; C. Chen, Phys. Rev. **D85**, 034007 (2012);
- [49] T. Plehn, G.P. Salam, M. Spannowsky, Phys. Rev. Lett. **104**, 111801 (2010); G.D. Kribs, A. Martin, T.S. Roy *et al.*, Phys. Rev. **D81**, 111501 (2010); D.E. Soper, M. Spannowsky, JHEP **1008**, 029 (2010); C.-R. Chen, M.M. Nojiri, W. Sreethawong, JHEP **1011**, 012 (2010); A. Falkowski *et al.*, Phys. Rev. **D84**, 074022 (2011); G.D. Kribs, A. Martin, T.S. Roy and M. Spannowsky, Phys. Rev. **D82**, 095012 (2010); C. Hackstein and M. Spannowsky, Phys. Rev. **D82**, 113012 (2010); B. Bellazzini, C. Csaki, J. Hubisz and J. Shao, Phys. Rev. **D83**, 095018 (2011); D.E. Soper and M. Spannowsky, Phys. Rev. **D84**, 074002 (2011); Y. Bai and J. Shelton, arXiv:1107.3563 [hep-ph]; J.R. Walsh and S. Zuberi, arXiv:1110.5333 [hep-ph]; L.G. Almeida *et al.*, arXiv:1112.1957 [hep-ph];
- [50] S. Yang and Q.-S. Yan, JHEP **1202**, 074 (2012) arXiv:1111.4530 [hep-ph].
- [51] J.M. Butterworth, J.R. Ellis, A.R. Raklev and G.P. Salam, Phys. Rev. Lett. **103**, 241803 (2009) arXiv:0906.0728 [hep-ph].
- [52] T. Sjostrand, S. Mrenna and P.Z. Skands, JHEP **0605**, 026 (2006) arXiv:hep-ph/0603175.
- [53] M. Cacciari and G.P. Salam, Phys. Lett. **B641**, 57 (2006) arXiv:hep-ph/0512210; M. Cacciari, G.P. Salam and G. Soyez, arXiv:1111.6097 [hep-ph].
- [54] Y.L. Dokshitzer, G.D. Leder, S. Moretti and B.R. Webber, JHEP **9708**, 001 (1997) [hep-ph/9707323]; M. Wobisch and T. Wengler, In *Hamburg 1998/1999, Monte Carlo generators for HERA physics*, p. 270, hep-ph/9907280.
- [55] M. Dasgupta, L. Magnea and G.P. Salam, JHEP **0802**, 055 (2008) arXiv:0712.3014 [hep-ph].
- [56] See, for example, CMS note CMS-PAS-BTV-11-001 (2011).
- [57] A. Pukhov, hep-ph/0412191.
- [58] CTEQ Collaboration, H.L. Lai *et al.*, Eur. Phys. J. **C12**, 375, arXiv:hep-ph/9903282.
- [59] T. Yetkin *et al.* [CMS Collaboration], Acta Phys. Polon. **B38**, 661 (2007).